

## N, B, Si-tridoped mesoporous TiO<sub>2</sub> with high surface area and excellent visible-light photocatalytic activity

Chenxu He · Baozhu Tian · Jinlong Zhang

Received: 27 November 2009 / Accepted: 28 January 2010 / Published online: 15 June 2010  
© Springer Science+Business Media B.V. 2010

**Abstract** N, B, Si-tridoped mesoporous TiO<sub>2</sub>, together with N-doped, N, B-codoped and N, Si-codoped TiO<sub>2</sub>, was prepared by a modified sol–gel method. The samples were characterized by wide-angle X-ray diffraction (WAXRD), N<sub>2</sub> adsorption–desorption, transmission electron microscopy (TEM), Fourier transform infrared (FT-IR) spectroscopy, UV–visible adsorbance spectra (UV–vis) and X-ray photoelectron spectra (XPS). The N, B, Si-tridoped mesoporous TiO<sub>2</sub> showed small crystallite size, large specific surface area (350 m<sup>2</sup>/g), uniform pore distribution (3.2 nm) and strong absorption in the visible light region. The photocatalytic activities of the samples were evaluated by the photodegradation of 2,4-dichlorophenol (2,4-DCP) aqueous solution. The N, B, Si-tridoping sample exhibited much higher photocatalytic activity compared with other synthesized photocatalysts. The high activity could be attributed to the strong absorption in the visible light region, large specific surface area, small crystallite size, large amount of surface hydroxyl groups, and mesoporosity.

**Keywords** Mesoporous · TiO<sub>2</sub> · N, B, Si-tridoped · High surface area · Photocatalyst

---

C. He · B. Tian · J. Zhang

Key Laboratory for Advanced Materials and Institute of Fine Chemicals, East China University of Science and Technology, 130 Meilong Road, 200237 Shanghai, People's Republic of China

J. Zhang (✉)

School of Chemistry and Materials Science, Guizhou Normal University, 550001 Guiyang, People's Republic of China  
e-mail: jlzhang@ecust.edu.cn

## Introduction

In the last decade, mesoporous materials have attracted intense interest for their applications in solar cells, catalysts, sensors, and so on. Among them, mesoporous  $\text{TiO}_2$ , as one of the most promising photocatalysts, has been widely investigated due to its advantages such as high specific surface area, high efficiency, good chemical stability, and nontoxicity [1, 2]. Many efforts have been devoted to prepare mesoporous  $\text{TiO}_2$  for applications. However, it should be pointed out that there were two issues which restrict its practical applications.

One was that the crystallinity of the mesoporous  $\text{TiO}_2$  framework was usually not satisfied, and titania mesostructures had such poor thermal stability that calcination treatment often results in the collapse of mesostructure. The collapse was believed to be caused by the intrinsical crystallization of amorphous  $\text{TiO}_2$  into anatase phase and crystal growth during calcinations [3, 4]. With the purpose of improving the thermal stability of mesostructure  $\text{TiO}_2$ , a widespread method was to incorporate another inorganic oxide such as  $\text{SiO}_2$  [5, 6],  $\text{Al}_2\text{O}_3$ ,  $\text{ZrO}_2$ , and  $\text{WO}_3$  [7] into the mesostructured  $\text{TiO}_2$  frameworks. Among these inorganic oxides,  $\text{SiO}_2$  was widely investigated. The addition of  $\text{SiO}_2$  can not only improve the thermal stability by inhibiting the crystalline growth and phase transformation but also increase the surface area and surface acidity [8]. However, the incorporation of  $\text{SiO}_2$  usually leads to poor crystallinity, and the photocatalytic application was restricted.

Another issue was that only UV light can be used for photocatalytic reaction, due to the large bandgap of  $\text{TiO}_2$  (3.0–3.2 eV). In order to utilize a wider range of the solar light, many studies on the physical [9–14] and chemical doping [18–22] modification of  $\text{TiO}_2$  to enable the absorption of visible light for reactions under visible light irradiation have been presented. Transition metal ions such as Cr and V [9–17] and nonmetal dopants such as N [18], B [19], S [20], C [21], and F [22] have also attracted intense interest. Among those doped materials, N-doped  $\text{TiO}_2$  was considered to be an efficient photocatalyst for decreasing the band gap and extending the visible light photoresponse of  $\text{TiO}_2$ . However, N-doped  $\text{TiO}_2$  often leads to very limited visible light activity [23]. In order to further enhance the visible light activity of the N-doped  $\text{TiO}_2$ , nonmetal elements codoped  $\text{TiO}_2$  such as B and N [24, 25], S and N [26], C and N [27], and F and N [28] have been recently studied. However, to our knowledge, there has been no report on the preparation of N, B and Si-tridoped mesoporous  $\text{TiO}_2$ .

In the present study, we explored a modified sol-gel method for the preparation of N, B and Si-tridoped mesoporous  $\text{TiO}_2$ . In this method, we prepared a  $\text{TiO}_2\text{-SiO}_2$  sol which initially contained nanocrystalline particles, then the nanocrystalline particles were used as the assembly units to prepare mesoporous  $\text{TiO}_2$  using dodecylamine as surfactant template. Therefore, the samples possess high surface area and good crystallinity. Herein, silica was introduced as a mesostructure stabilizer. Dodecylamine not only acted as a pore template but also as a nitrogen dopant. And  $\text{H}_3\text{BO}_3$  acted as a boron dopant which could further enhance visible-light activity. The synergistic effect of dopants on their photocatalytic activities was investigated.

## Experimental

### Preparation of samples

In this study, tetrabutyl titanate ( $\text{Ti}(\text{OC}_4\text{H}_9)_4$ , TBOT) and dodecylamine (DDA) were chemical pure, and the other chemicals were analytic pure. All chemicals were used without further purification. In a typical synthesis, 30 mL TBOT was mixed with 1.94 mL tetraethyl orthosilicate ( $\text{Si}(\text{OC}_2\text{H}_5)_4$ , TEOS) and 2 mL anhydrous ethanol under stirring (solution A). Meanwhile, 0.16 g boric acid ( $\text{H}_3\text{BO}_3$ ) and 1.5 mL  $\text{HNO}_3$  were dissolved in 150 mL distilled water under stirring (solution B). Then solution A was added dropwise into solution B with vigorous stirring under room temperature. The resulting white precipitation was subsequently refluxed at 60 °C for 3 h. The hydrolysis products were two layers of solution, the transparent sol was separated from the solution and 8.82 g DDA was added into the sol under vigorous stirring. The reaction solution was kept stirring for an hour and then aged at 80 °C for 24 h in a closed flask. The resulting sol was transferred to a Petri dish, dried at 80 °C for 1 day and 100 °C for another day to give a yellow xerogel. Finally, the xerogel was calcined in sufficient air at 400 °C for 4 h to get a yellow sample. N–TiO<sub>2</sub>, N, B–TiO<sub>2</sub> and N, Si–TiO<sub>2</sub> were prepared by the same method as for N, B, Si–TiO<sub>2</sub>, except that N–TiO<sub>2</sub> without TEOS and  $\text{H}_3\text{BO}_3$ , N, B–TiO<sub>2</sub> without TEOS, and N, Si–TiO<sub>2</sub> without  $\text{H}_3\text{BO}_3$ .

### Characterization methods

Wide-angle X-ray diffraction (WAXRD) patterns of all samples were collected in  $\theta$ – $2\theta$  mode using Rigaku D/MAX-2550 diffractometer ( $\text{Cu K}_{\alpha 1}$  radiation,  $\lambda = 1.5406 \text{ \AA}$ ), operated at 40 kV and 100 mA. The crystallite size was estimated by applying the Scherrer equation to the FWHM of the (101) peak of anatase, with  $\alpha$ -silicon (99.9999%) as a standard for the instrumental line broadening. The porous structures of the samples have been measured using the BET method by nitrogen adsorption–desorption isotherms at –196 °C. Before measurement, the samples were evacuated overnight at 200 °C. By using a Micromeritics ASAP 2000 system, the BET and BJH methods were applied for the determination of the specific surface area, and the mean mesoporous equivalent diameter, respectively. The porous structures were also observed by a 2100 JEOL high-resolution transmission electron microscopy (HRTEM) at 200 kV. Fourier transform infrared (FT-IR) spectra were recorded on a Nicolet Magna 380 spectrometer. UV–vis diffuse reflectance spectra (DRS) were obtained with a Scan UV–vis-NIR spectrophotometer (Varian Cary 500) equipped with an integrating sphere assembly using polytetrafluoroethylene as reflectance sample. X-ray photoelectron spectroscopy (XPS) was recorded with a Shimadzu ESCA-3200 spectrometer using a radiation source of  $\text{Mg K}_{\alpha}$  radiation with the energy of 1,253.6 eV, 30 mA × 8 kV. The shift of the binding energy due to relative surface charging was corrected using the C1s level at 284.8 eV as an internal standard.

## Photocatalytic measurement

2,4-Dichlorophenol (2,4-DCP) was chosen as model pollutant to evaluate the photocatalytic activity of obtained samples. Typically, 0.08 g of the sample was dispersed in 80 mL of 30 mg/L 2, 4-dichlorophenol aqueous solution using a 100-mL capacity glass tube. After being stirred in dark for 30 min to reach the adsorption equilibrium, the solution was then irradiated with a 1,000-W halogen lamp which was filtered by a 420-nm cut-off filter. The distance between the lamp and the reaction tube was fixed at 10 cm. At regular irradiation intervals, 4 mL suspension was taken out and centrifuged. The clear centrifugate was measured for checking the residual concentration of 2,4-dichlorophenol ( $\lambda = 284$  nm) with a UV-vis spectrophotometer (Varian Cary 100).

## Results and discussion

### Structure and properties of samples

Figure 1 shows the effects of Si and B dopants on the phase structures of the samples. It can be seen that the sample without adding TEOS and  $H_3BO_3$  (Fig. 1a) is composed of anatase and a small amount of rutile and brookite phases. However, the rutile and brookite phases disappear when TEOS is added (Fig. 1c, d), which implies that the introduction of Si dopant can inhibit the crystallization of brookite and the phase transformation of anatase-to-rutile. The sample with just the addition of  $H_3BO_3$  consists of anatase and brookite phases, but no rutile phase (Fig. 1b). This result indicates that B dopant can also inhibit the anatase-to-rutile phase transformation, but they cannot suppress the formation of brookite phase, which is consistent with previous reports [29, 30]. With the addition of  $H_3BO_3$ , the anatase peaks gradually become a little bit wider, indicating that B dopant can reduce the crystallite size of  $TiO_2$ . The anatase size of the samples are calculated based on the Scherrer–Debye formula and listed in Table 1. The effect of B dopant on the  $TiO_2$  crystallite size is a little weaker than that of Si dopant, and Si dopant is the main reason that inhibits the crystalline growth and phase transformation. It should be noted that no  $SiO_2$  or  $B_2O_3$  phases are detected in any of the WAXRD patterns. This is probably because the content of doping silica and boron is very slow, and they are well dispersed in the  $TiO_2$  framework.

The  $N_2$  adsorption–desorption isotherms of the samples are shown in Fig. 2. All the samples show type-IV isotherms, which are representative of mesoporous materials according to the IUPAC classification. The isotherms display a H2 hysteresis loop with a triangular shape which indicates that the samples have ink-bottle-shaped or cage-type pores [31, 32]. It can be calculated that the surface areas of Si-doped samples are larger than  $300\text{ m}^2/\text{g}$  and the average diameters of pores are both around 3.2 nm. The samples N– $TiO_2$  and N, B– $TiO_2$  have much smaller surface areas and larger pore diameters, due to the collapse of mesostructures. Moreover, the samples N, Si– $TiO_2$  and N, B, Si– $TiO_2$  have remarkable high adsorption at low relative pressure region (curves c and d in Fig. 2A), suggesting the

**Fig. 1** Wide-angle XRD patterns of the samples:  
*a* N–TiO<sub>2</sub>, *b* N, B–TiO<sub>2</sub>,  
*c* N, Si–TiO<sub>2</sub>, *d* N, B, Si–TiO<sub>2</sub>

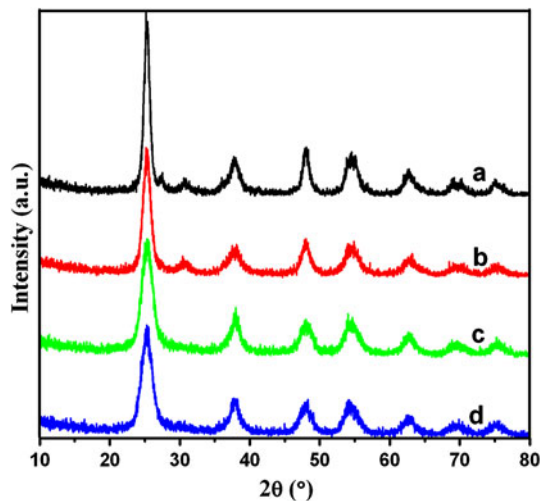


**Table 1** Structure parameters of the samples

Sample	Phase	$D_A^a$ (nm)	$D_{BJH}^b$ (nm)	$V_{BJH}^b$ (cm <sup>3</sup> /g)	$S_{BET}^b$ (m <sup>2</sup> /g)
N–TiO <sub>2</sub>	A, R, B	9.7	4.0	0.12	94
N, B–TiO <sub>2</sub>	A, B	6.8	3.9	0.22	144
N, Si–TiO <sub>2</sub>	A	5.5	3.2	0.21	312
N, B, Si–TiO <sub>2</sub>	A	5.5	3.2	0.24	350

<sup>a</sup> Average anatase crystallite size of TiO<sub>2</sub> was evaluated from Scherrer equation

<sup>b</sup> Average pore size ( $D_{BJH}$ ), pore volume ( $V_{BJH}$ ) and BET surface area ( $S_{BET}$ ) were estimated by nitrogen adsorption volume

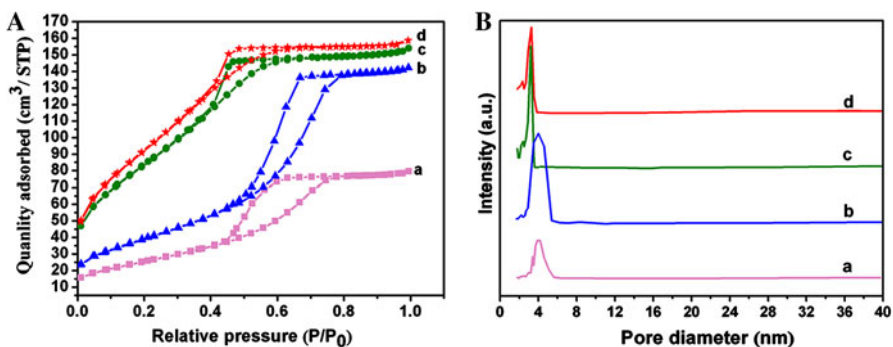


**Fig. 2** N<sub>2</sub> adsorption–desorption isotherms (a) and pore-size distributions of the samples (b): *a* N–TiO<sub>2</sub>, *b* N, B–TiO<sub>2</sub>, *c* N, Si–TiO<sub>2</sub>, *d* N, B, Si–TiO<sub>2</sub>

presence of micropores [33]. However, micropores cannot be detected in the samples N–TiO<sub>2</sub> and N, B–TiO<sub>2</sub>. The micropores may make a big contribution to the specific surface area of the samples N, Si–TiO<sub>2</sub> and N, B, Si–TiO<sub>2</sub>.

Figure 3 shows the transmission electron microscopy (TEM) images of the samples N–TiO<sub>2</sub> and N, B, Si–TiO<sub>2</sub>. It can be seen that the sample N–TiO<sub>2</sub> shows an irregular pore structure with large particles, and that the sample N, B, Si–TiO<sub>2</sub> exhibits wormhole-like mesostructure with littler particles. This result indicates that B and Si dopant can stabilize mesostructures and inhibit the aggregation of particles. From the HRTEM image (Fig. 3b, d), it can be observed that the crystalline size of N–TiO<sub>2</sub> ( $\sim 10$  nm) is much larger than that of N, B, Si–TiO<sub>2</sub> ( $\sim 6$  nm). This result is accordance with the WAXRD data. It is confirmed that N, B, Si-tridoping can significantly suppress the growth of crystal.

FT-IR spectra of the doped samples are shown in Fig. 4. The broad peak at around  $3,400\text{ cm}^{-1}$  corresponds to the surface adsorbed water and hydroxyl groups, and the peak at about  $1,630\text{ cm}^{-1}$  is due to the bending vibrations of O–H bonds [34]. It can be observed that the intensity of the above two peaks increases with Si and/or B doping, which indicates the Si and/or B dopant can effectively restrain the loss of surface hydroxyl groups during calcination. As a result, the hydroxyl groups on the surface of the samples can be preserved, which is a benefit for the photocatalytic reaction. The peak at around  $1,380\text{ cm}^{-1}$  that presents in the B-doped samples (Fig. 4b, d) indicates tri-coordinated boron in the framework [35, 36],

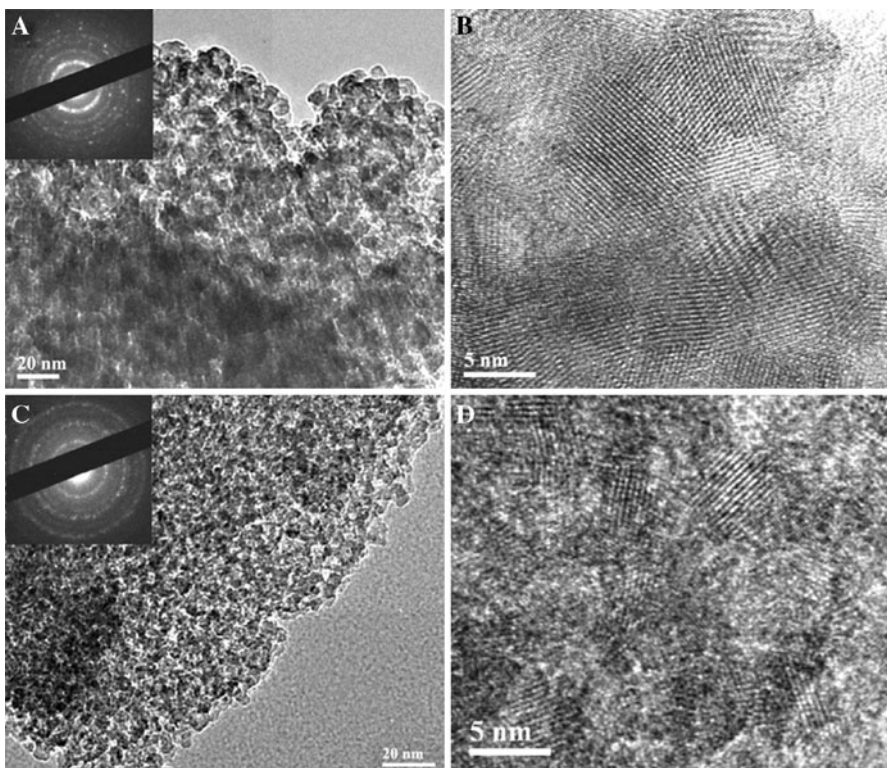
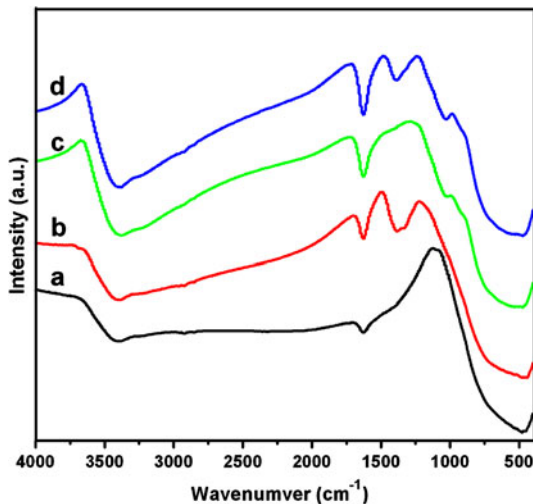


**Fig. 3** TEM and HRTEM images of the samples: **a, b** N–TiO<sub>2</sub>, **c, d** N, B, Si–TiO<sub>2</sub>. Insets in (a) and (c) is selected-area electron diffraction pattern obtained on the image area

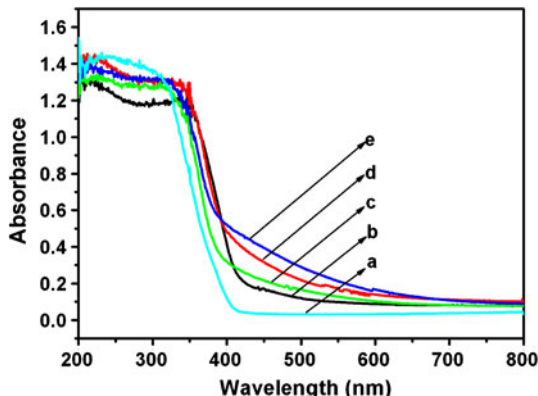
**Fig. 4** FT-IR spectra of the samples: *a* N–TiO<sub>2</sub>, *b* N, B–TiO<sub>2</sub>, *c* N, Si–TiO<sub>2</sub>, *d* N, B, Si–TiO<sub>2</sub>



which may be attributed to Ti–O–B bonds. Another peak around 1,200 cm<sup>-1</sup> is present in the N, Si–TiO<sub>2</sub> sample but absent for the N, B–TiO<sub>2</sub> sample. Thus, it can be assigned to the asymmetrical vibration of the Si–O–Si bonds in the bulk SiO<sub>2</sub> instead of the B–O bonds in the B<sub>2</sub>O<sub>3</sub> bulk [29, 36, 37]. The ambiguous peak at around 930 cm<sup>-1</sup> for the samples N, Si–TiO<sub>2</sub> and N, B, Si–TiO<sub>2</sub>, which is difficult to be observed, belongs to the asymmetric stretching vibration of the Ti–O–Si bonds [33]. The Ti–O–Si bonds are very weak possibly due to the small amount of SiO<sub>2</sub> dopant.

Figure 5 shows the UV–vis diffuse reflectance spectra of the samples compared with commercial P25 photocatalyst. It is apparent that the adsorption of P25 is limited only to ultraviolet light region, whereas all the synthesized samples are significantly extended to the visible range. With the introduction of a small amount of nitrogen, the adsorption of the samples N–TiO<sub>2</sub> and N, Si–TiO<sub>2</sub> shifts to visible region due to the forming of a dopant energy level above the valence band of TiO<sub>2</sub>.

**Fig. 5** UV–vis absorption spectra of the samples *b* N–TiO<sub>2</sub>, *c* N, Si–TiO<sub>2</sub>, *d* N, B–TiO<sub>2</sub>, *e* N, B, Si–TiO<sub>2</sub> compared with *a* P25



[38]. And the absorption intensity in the visible light region of N, Si–TiO<sub>2</sub> is stronger than that of N–TiO<sub>2</sub>, because N, Si–TiO<sub>2</sub> has more hydroxyl groups that can preserve more N species. As the introduction of boron, the absorption band at the visible region becomes more apparent (Fig. 5d, e), which is in agreement with the previous reports [16, 24, 30]. However, after the doping of SiO<sub>2</sub>, the samples show a blue shift of absorption edge (Fig. 5c, e) compared with the undoped samples, which should be ascribed to the decrease of TiO<sub>2</sub> crystal size. When the SiO<sub>2</sub> is doped, the crystal size of TiO<sub>2</sub> is less than 10 nm, which can cause quantum size effect and result in band gap widening [6].

Figure 6 shows the high resolution XPS spectra of N–TiO<sub>2</sub> and N, B, Si–TiO<sub>2</sub> for N 1s. Two peaks at around 400.2 and 396.0 eV can be observed in the sample N–TiO<sub>2</sub>. The former peak is attributed to N species chemisorbed on the surface [39], and the latter is assigned to substitutional N in O–Ti–N linkages [40]. Both the chemisorbed N species and substitutional N can contribute to visible light absorption. For the sample N, B, Si–TiO<sub>2</sub>, the two peaks are shown at 400.8 and 396.7 eV, respectively, which moves toward larger binding energy in comparison of that of N–TiO<sub>2</sub>. The shift in the binding energy of electrons can be ascribed to the doping B<sup>3+</sup> in TiO<sub>2</sub> lattice [41].

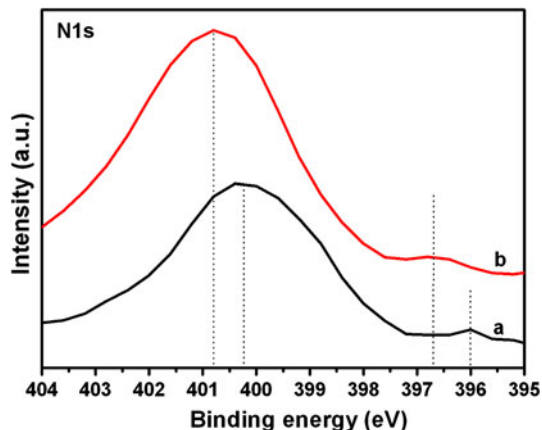
Figure 7a shows the B1s XPS spectra of N, B, Si–TiO<sub>2</sub>. It can be observed that the B 1s region contains only one peak at 191.6 eV. This peak is attributed to O–Ti–B bonds, which contributes to additional visible light absorption [25, 30]. This result confirms that part of B atoms are incorporated into TiO<sub>2</sub>.

The O1s XPS spectra of the sample N, B, Si–TiO<sub>2</sub> are wide and asymmetric (Fig. 7b), and can be fitted to three peaks at 529.6, 531.2 and 533.0 eV. The peaks at 529.6, 531.2 eV can be attributed to Ti–O–Ti, Ti–O–Si bonds, respectively [42, 43]. Another peak at 533.0 eV may be attributed to Si–O–Si and B–O bonds [42–44].

### Activity of photocatalysts

The photocatalytic activities of the different samples were investigated by detecting the decomposition ratios of 2,4-DCP aqueous solution under visible light

**Fig. 6** XPS spectra of N 1s in the samples *a* N–TiO<sub>2</sub>, *b* N, B, Si–TiO<sub>2</sub>



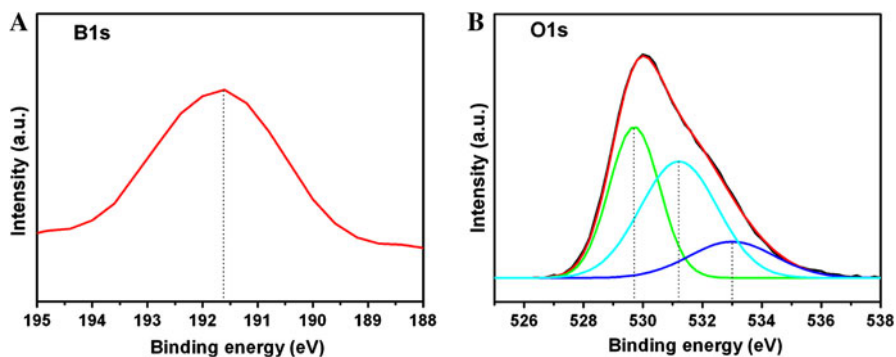
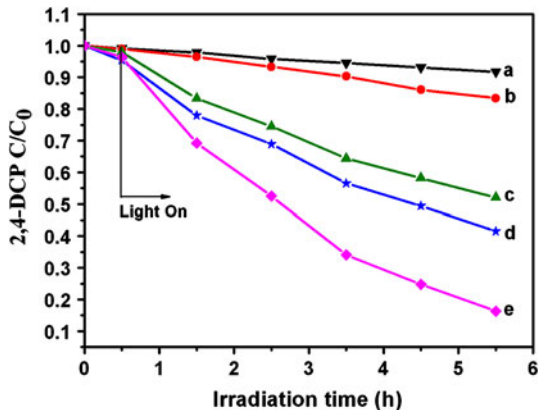


**Fig. 7** XPS spectra of B 1s and O 1s in the sample N, B, Si-TiO<sub>2</sub>

illumination. The activity of commercial Degussa P25 was carried out under the identical conditions for comparison.

Compared to P25, which is almost nonactive under visible light irradiation, all the obtained samples exhibit much better photocatalytic activity (Fig. 8). Among the samples, the photocatalytic activity of N, B-TiO<sub>2</sub>, N, Si-TiO<sub>2</sub> and N, B, Si-TiO<sub>2</sub> is much superior to that of N-TiO<sub>2</sub>. And the sample N, B, Si-TiO<sub>2</sub> shows the highest photocatalytic activity, which is fivefold more than that of N-TiO<sub>2</sub>, and almost double than that of N, B-TiO<sub>2</sub>. The high photocatalytic activity of N, B, Si-TiO<sub>2</sub> can be attributed to several factors. Firstly, N, B, Si-tridoping can enhance the absorption intensity of the sample in the visible region, which is benefit for the sample receiving more photons and producing more photogenerated electrons and holes. In addition, B dopant in the sample can eliminate the oxygen vacancies produced by N dopant and reduce the electron–hole recombination centers [45]. Secondly, it has a large surface area and pore volume. Photocatalytic reaction is a surface-based reaction, thus large surface area usually promotes the reaction rate because it can supply more adsorption sites and photocatalytic reaction centers [1]. Moreover, the sample preserves mean mesoporous channels. As the hydroxyl

**Fig. 8** Photocatalytic activity of the samples *b* N-TiO<sub>2</sub>, *c* N, B-TiO<sub>2</sub>, *d* N, Si-TiO<sub>2</sub>, *e* N, B, Si-TiO<sub>2</sub> compared with *a* P25 under visible light irradiation



radicals ( $\cdot\text{OH}$ ) generated on the  $\text{TiO}_2$  surface can hardly diffuse out of the mesopores [46], then the  $\cdot\text{OH}$  can attack the 2,4-DCP molecules effectively inside the pores, resulting in the high photocatalytic activity. Thirdly, the sample has a small particle size. It has been reported that the average transfer time of photo-generated electrons and holes on small particle  $\text{TiO}_2$  is obviously shorter than that of larger particles [47]. Therefore, the recombination rate of electrons and holes will decrease, which is beneficial for the photocatalytic activity. Fourthly, the sample possesses more surface hydroxyl groups than the other samples. And the surface hydroxyl groups can capture the photogenerated holes, produce active hydroxyl radicals, and prevent electron–hole recombination during the photocatalytic reaction [8]. Thus, it exhibits an excellent visible light photocatalytic activity.

## Conclusions

The N, B, Si-tridoped mesoporous  $\text{TiO}_2$  photocatalyst can be prepared by a modified sol–gel method. The N, B, Si-tridoping sample had good mesoporous stability and good crystallinity at the same time. Moreover, it showed a strong absorption in the visible light region because the doping of N and/or B resulted in a narrower band gap. The sample had small crystallite size, large specific surface area, and uniform pore distribution. In this method, both the B and Si dopants could suppress the growth of crystallite size and inhibit anatase-to-rutile phase transformation. However, the Si dopant had a more significant effect on the crystal structure. N, B-codoping and N, Si-codoping obviously enhance the photocatalytic activity of  $\text{TiO}_2$  photocatalysts. And the N, B, Si-tridoped  $\text{TiO}_2$  showed the highest activity, which could be attributed to the strong absorption in the visible light region, large specific surface area, mesoporosity, small crystallite size, and preserved surface hydroxyl group.

**Acknowledgments:** This work has been supported by National Nature Science Foundation of China (20773039, 20977030); National Basic Research Program of China (973 Program, 2007CB613301, 2010CB732306), and the Ministry of Science and Technology of China (2006AA06Z379, 2006DFA52710).

## References

1. M.R. Hoffman, S.T. Martin, W. Choi, D.W. Bahnemann, *Chem. Rev.* **95**, 69 (1995)
2. A. Fujishima, T.N. Rao, D.A. Tryk, *J. Photochem. Photobiol. C: Photochem. Rev.* **1**, 1 (2000)
3. D.L. Li, H.S. Zhou, I. Honma, *Nat. Mater.* **3**, 65 (2004)
4. D. Fattakhova-Rohlfing, M. Wark, T. Brezesinski, B.M. Smarsly, J. Rathouský, *Adv. Funct. Mater.* **17**, 123 (2007)
5. W.Y. Dong, Y.J. Sun, C.W. Lee, W.M. Hua, X.C. Lu, Y.F. Shi, S.C. Zhang, J.M. Chen, D.Y. Zhao, *J. Am. Chem. Soc.* **129**, 13894 (2007)
6. G. Calleja, D.P. Serrano, R. Sanz, P. Pizarro, *Microporous Mesoporous Mater.* **111**, 429 (2008)
7. M.J. Yuan, Z. Shan, B.Z. Tian, B. Tu, P.Y. Yang, D.Y. Zhao, *Microporous Mesoporous Mater.* **78**, 37 (2005)
8. X.Z. Fu, L.A. Clark, Q. Yang, M.A. Anderson, *Environ. Sci. Technol.* **30**, 647 (1996)
9. M. Anpo, Y. Ichihashi, M. Takeuchi, H. Yamashita, *Stud. Surf. Sci. Catal.* **121**, 305 (1998)

10. M. Anpo, Stud. Surf. Sci. Catal. **130**, 157 (2000)
11. M. Anpo, Pure Appl. Chem. **72**, 1787 (2000)
12. H. Yamashita, M. Harada, J. Misaka, M. Takeuchi, Y. Ichihashi, F. Goto, M. Ishida, T. Sakai, M. Anpo, J. Synchrotron Radiat. **8**, 569 (2001)
13. M. Anpo, S. Kishiguchi, Y. Ichihashi, M. Takeuchi, H. Yamashita, K. Ikeue, B. Morin, A. Davidson, M. Che, Res. Chem. Intermed. **27**, 459 (2001)
14. J. Zhou, M. Takeuchi, A.K. Ray, M. Anpo, X.S. Zhao, J. Colloid Interface Sci. **311**, 497 (2007)
15. M. Anpo, M. Takeuchi, K. Ikeue, S. Dohshi, Curr. Opin. Solid State Mater. Sci. **6**, 381 (2002)
16. M. Anpo, M. Takeuchi, J. Catal. **216**, 505 (2003)
17. M. Anpo, Bull. Chem. Soc. Jpn. **77**, 1427 (2004). (and references therein)
18. R. Asahi, T. Morikawa, T. Ohwaki, K. Aoki, Y. Taga, Science **293**, 269 (2001)
19. W. Zhao, W.H. Ma, C.C. Chen, J.C. Zhao, Z.G. Shuai, J. Am. Chem. Soc. **126**, 4782 (2004)
20. T. Umebayashi, T. Yamaki, H. Itoh, K. Asai, Appl. Phys. Lett. **81**, 454 (2002)
21. C. Di Valentin, G. Pacchioni, A. Selloni, Chem. Mater. **17**, 6656 (2005)
22. J.C. Yu, J.G. Yu, W.K. Ho, Z.T. Jiang, L.Z. Zhang, Chem. Mater. **14**, 3808 (2002)
23. H. Irie, Y. Watanabe, K. Hashimoto, J. Phys. Chem. B **107**, 5483 (2003)
24. S. In, A. Orlov, R. Berg, F. García, S. Pedrosa-Jimenez, M.S. Tikhov, D.S. Wright, R.M. Lambert, J. Am. Chem. Soc. **129**, 13790 (2007)
25. N.O. Gopal, H.H. Lo, S.C. Ke, J. Am. Chem. Soc. **130**, 2760 (2008)
26. X. Li, R.C. Xiong, G. Wei, Catal. Lett. **125**, 104 (2008)
27. Y. Ao, J.J. Xu, D.G. Fu, C.W. Yuan, Microporous Mesoporous Mater. **118**, 382 (2009)
28. X. Du, J.H. He, Y.Q. Zhao, J. Phys. Chem. C **113**, 14151 (2009)
29. D. Chen, D. Yang, Q. Wang, Z.Y. Jiang, Ind. Eng. Chem. Res. **45**, 4110 (2006)
30. G. Liu, Y.N. Zhao, C.H. Sun, F. Li, G.Q. Lu, H.M. Cheng, Angew. Chem. Int. Ed. **47**, 4516 (2008)
31. S.Y. Choi, M. Mamak, N. Coombs, N. Chopra, G.A. Ozin, Adv. Funct. Mater. **14**, 335 (2004)
32. C.X. He, B.Z. Tian, J.L. Zhang, Microporous Mesoporous Mater. **126**, 50 (2009)
33. K.G.K. Warrier, S. Rajesh Kumar, C.P. Sibu, J. Porous. Mater. **8**, 311 (2001)
34. J. Rubio, J.L. Oteo, M. Villegas, P. Duran, J. Mater. Sci. **32**, 643 (1997)
35. T. On, S. Kaliaguine, L. Bonneviot, J. Catal. **157**, 23 (1995)
36. K.Y. Jung, S.B. Park, S.K. Ihm, Appl. Catal. B: Environ. **51**, 239 (2004)
37. R.J. Davis, Z.F. Liu, Chem. Mater. **9**, 2311 (1997)
38. X.F. Qiu, C. Burda, Chem. Phys. **339**, 1 (2007)
39. H. Mariag, A. Miguelpelaez, A. Delacruz, J. Shoemaker, A. Dionysiou, Environ. Sci. Technol. **41**, 7530 (2007)
40. X. Yang, C. Cao, L. Erickson, K. Hohn, R. Maghirang, K. Klabunde, J. Catal. **260**, 128 (2008)
41. Y. Li, G. Ma, S. Peng, G. Lu, S. Li, Appl. Surf. Sci. **254**, 6831 (2008)
42. Z.L. Hua, J.L. Shi, L.X. Zhang, M.L. Ruan, J.N. Yan, Adv. Mater. **14**, 830 (2002)
43. H. Zhang, X. Luo, J. Xu, B. Xiang, D. Yu, J. Phys. Chem. B **108**, 14866 (2004)
44. N. Lu, X. Quan, J.Y. Li, S. Chen, H.T. Yu, G.H. Chen, J. Phys. Chem. C **111**, 11836 (2007)
45. T. Ihara, M. Miyoshi, Y. Iriyama, O. Matsumoto, S. Sugihara, Appl. Catal. B **42**, 403 (2003)
46. Y. Shiraishi, N. Saito, T. Hirai, J. Am. Chem. Soc. **127**, 12820 (2005)
47. T. Tong, J. Zhang, B. Tian, F. Chen, D. He, J. Hazard. Mater. **155**, 572 (2008)